

Towards a unified shear-induced lift model for prolate spheroidal particles moving in arbitrary non-uniform flow

Yan Cui^a, Jure Ravnik^b, Matjaž Hriberšek^b, Paul Steinmann^{a,c,*}

^a Chair of Applied Mechanics, Friedrich-Alexander Universität Erlangen-Nürnberg, Paul-Gordan-Str. 3, Erlangen D-91052, Germany

^b Faculty of Mechanical Engineering, University of Maribor, Smetanova 17, Maribor, SI-2000, Slovenia

^c Glasgow Computational Engineering Centre, University of Glasgow, Glasgow, UK

ARTICLE INFO

Article history:

Received 30 April 2019

Revised 27 August 2019

Accepted 9 October 2019

Available online 11 October 2019

Keywords:

Prolate spheroidal particle

Unified shear-induced lift

Saffman-type lift

Lagrangian particle tracking

ABSTRACT

The paper proposes a unified shear-induced lift force model which divides the lift force into four lift components arising from the spin tensor, the volumetric and the deviatoric parts of the rate of deformation tensor, and the inertia effect of the Stokes drag. This unified model is successfully simplified into a shear-induced lift model for prolate spheroidal particles moving in arbitrary flow conditions via analogy arguments. The simplified shear-induced lift model for prolate spheroidal particles is verified by comparing it with several established lift force models via simulation of a prolate spheroidal particle moving in the Poiseuille and lid-driven cavity flows. The computational results demonstrate that the present lift force model for prolate spheroidal particles is applicable in flow cases with streamwise and non-streamwise flow shear. The implementation of the simplified lift model leads to computational results with reasonably small difference to the results of the full lift model of Cui et al. [*Int. J. Multiph. Flow*, **111**, 232–240 (2019)], with a significantly decreased computational cost, rendering it as suitable for the implementation in large scale Lagrangian particle tracking.

© 2019 Elsevier Ltd. All rights reserved.

1. Introduction

The shear-induced lift force acting on particles moving at small, but finite Reynolds number (i.e. the so-called Saffman-type lift) has been studied for several decades [4,6,7,9–12,14,15,18–23,26,27,32,36].

In the case of spherical particles, Saffman [26,27] first investigated a sphere moving through a highly viscous liquid in a simple shear flow and calculated the lift force at small, but finite Reynolds numbers via singular perturbation methods. Saffman's calculation has been shown to be in a good agreement with experiments [33,34] and remains significant also today [32]. Crowe et al. [6] extended the Saffman lift by generalising the simple shear flow to an arbitrary linear shear flow. However, Saffman-type lift has several restrictions, such as the particle moving in the unconfined flow, the particle Reynolds number $Re_p = D_p |\mathbf{u} - \mathbf{v}|/\nu \ll 1$ (where D_p is the particle diameter, $\mathbf{u} - \mathbf{v}$ is the slip velocity, and ν is

the fluid kinematic viscosity), the particle shear Reynolds number $Re_G = D_p^2 |\mathbf{G}|/\nu \ll 1$ (where \mathbf{G} is the velocity gradient tensor) and $Re_p \ll Re_G^{1/2}$. With these constraints, Saffman lift cannot be applied in most of the flow situations. McLaughlin [21] extended the Saffman's theory and successfully removed one of the Saffman assumptions, i.e. $Re_p \ll Re_G^{1/2}$. Bagchi and Balachandar [4] and Legendre and Magnaudet [18] calculated the lift force acting on a spherical particle and a bubble, respectively, in a viscous linear shear flow over a wide range of Reynolds number values (i.e. $0.1 \leq Re_p \leq 500$) and Legendre and Magnaudet [18] found that a small but consistent decrease of the lift coefficient occurs when the shear rate becomes large. Magnaudet [19] studied the influence of the wall effect on the shear-induced lift acting on a spherical drop. In [20] the deformation-induced migration of a buoyant drop was also studied. Although most of Magnaudet's studies focus on bubbles or drops, one can deduct some important findings also for particles. In recent years, there were many reports on the computation of the lift force acting on a particle by using Direct Numerical Simulation (DNS) [10,15–17,25]. Cui and Sommerfeld [10] calculated the lift force acting on a spherical particle sitting on a smooth plane wall by using Lattice Boltzmann Method (LBM) and found that the lift coefficient becomes a constant value of about 3

* Corresponding author at: Chair of Applied Mechanics, Friedrich-Alexander Universität Erlangen-Nürnberg, Paul-Gordan-Str. 3, D-91052 Erlangen, Germany.

E-mail addresses: yan.cui@fau.de (Y. Cui), jure.ravnik@um.si (J. Ravnik), matjaz.hribersek@um.si (M. Hriberšek), paul.steinmann@fau.de (P. Steinmann).

when the particle shear Reynolds number is less than 1. Jebakumar et al. [16] calculated the lift acting on a finite-sized particle moving in a wall-bounded flow by using the LBM and found that at low Stokes number the particle behaves like a neutrally buoyant particle and exhibits the Segré-Silberberg effect. In [17], LBM simulation of fully-resolved large particles (i.e. larger than the Kolmogorov scale) moving in a turbulent channel flow was performed.

In the case of non-spherical particles, the studies of shear-induced lift are far less numerous. Harper and Chang [14] found that particles in a Newtonian fluid adopt an orientation with respect to the maximum energy dissipation and generalised Saffman's calculation to three-dimensional (3D) bodies in a linear shear flow by introducing a lift tensor calculated via asymptotic methods. Fan and Ahmadi [11] initially applied Harper & Chang's calculation in the case of axisymmetric ellipsoidal particles. Feng and Kleinstreuer [12] generalised the lift model of [14], valid for a linear shear flow, to a complex shear flow by superimposing results for several pure shear flows based on the values of the extra-diagonal components of the velocity gradient tensor. A simple counter example [13] is given by the lift tensor obtained for a particle in a rotating fluid under the same assumptions as in Harper & Chang. In the case of a rarefied gas, based on the gas kinetic theory a lift model for axial symmetric particles moving in a linear shear flow was investigated by Wang et al. [36].

One of the key challenges of a shear-induced lift model for non-spherical particles is to derive a computational method which would allow the accurate computation of shear-induced lift forces acting on small non-spherical particles in a general fluid flow, i.e. would not be limited to a certain type of flow (e.g. linear shear flow), as is the case with all the previous derivations. In general, it is not possible to transform an arbitrary velocity gradient into a pure (linear) shear flow, since a rotational flow, or a pure deformational flow, have intrinsic properties that differ from each other and, in particular, differ from those of a pure shear flow. However, if the particle Reynolds number values considered are sufficiently small, it is reasonable to approximate the fluid flow around a particle as linear and dominated by viscous forces (creeping flow approximation). Cui et al. [7,9] proposed a generic method to extend the shear-induced lift force models that were originally devised for linear shear flow to arbitrary flow conditions by performing two coordinate rotations. This method is applied to the computation of the shear-induced lift force acting on a prolate spheroidal particle moving in arbitrary non-uniform flow. Cui et al. [7] (Part I of a two-part research work, abbr. Part I) calculated the lift force arising from the dominant streamwise flow shear. In [9] (abbr. Part II) the influence of the non-streamwise flow shear on the lift force was also taken into account. By assuming that the particle slip velocity is parallel to the fluid velocity along the particle trajectory, the lift force model for prolate spheroidal particle proposed in Part II is applicable in flow cases with streamwise and non-streamwise flow shear. In fluid flows which are dominated by the streamwise shear, the lift force model of Part I is slightly more accurate than the lift force model of Part II. However, the shear-induced lift force models proposed by Part I and II are numerically expensive since the calculation involves two coordinate rotations for each particle for every time step. The aim of the present work is therefore the development of a computationally more efficient yet acceptably accurate shear-induced lift force model for prolate spheroidal particles moving in an arbitrary non-uniform flow, directly applicable in the Lagrangian particle tracking.

In the present study, we restricted ourselves to the following four conditions:

1. The particle is moving in an unconfined flow, i.e. the influence of the wall effect on the shear-induced lift is not taken into account;

2. The particle is a Lagrangian point particle, i.e. the influence of the finite size effect on the shear-induced lift is not taken into account;
3. All Saffman's assumptions are kept;
4. The derivation is made from the standpoint of non-spherical shaped particles.

The third condition would limit the usage of the shear-induced lift model significantly, however in our previous studies [7,9] it was established that the Saffman's assumptions are usually valid for micro-sized particles. Therefore, the proposed shear-induced lift model could be applied in a wide range of applications, e.g. in drug delivery, sedimentation of sludge flocs, or concentration of fine particulate matter. The present study focuses only on the non-spherical shaped particle, without the aim to incorporate all the available lift-correction models for spherical particles from the scientific literature into the present shear lift model.

The paper is organized as follows. In Section 2, a unified shear-induced lift force model is proposed. By implementing analogy arguments, this unified model is then simplified based on the previous insights obtained for the case of prolate spheroidal particles [9]. In Section 3, the simplified unified shear-induced lift force model for prolate spheroidal particles is verified with respect to other lift force models for the case of the Poiseuille and lid-driven cavity flows.

Notation: Tensors of various order are expressed in bold italic font, i.e. a first-order tensor (vector) and a second-order tensor are denoted by \mathbf{A} and \mathbf{B} , respectively. In a Cartesian coordinate system with base vectors \mathbf{e}_i ($i = 1, 2, 3$) they have the coordinate representation $\mathbf{A} = A_i \mathbf{e}_i$ and $\mathbf{B} = B_{ij} \mathbf{e}_i \otimes \mathbf{e}_j$, respectively, whereby Einstein's summation convention applies for repeated indices. A_i and B_{ij} are the coefficients of \mathbf{A} and \mathbf{B} , respectively, in the chosen coordinate system \mathbf{e}_i . They may be arranged into coefficient matrices

$$\mathbf{A} := \begin{bmatrix} A_1 \\ A_2 \\ A_3 \end{bmatrix} \quad \text{and} \quad \mathbf{B} := \begin{bmatrix} B_{11} & B_{12} & B_{13} \\ B_{21} & B_{22} & B_{23} \\ B_{31} & B_{32} & B_{33} \end{bmatrix}$$

whereby bold non-italic font is used for coefficient matrices. Indeed \mathbf{A} is a column matrix, the superscript T denotes transposition so that $\mathbf{A}^T = [A_1, A_2, A_3]$ (a row matrix).

2. A unified shear-induced lift force model and its simplification

Particle transport in fluid flow is governed by the particle-fluid interaction, which is in the case of small particles typically accounted for within the Lagrangian particle tracking, where the kinematics equation and force balance equation in form of ordinary differential equations are solved along the particle trajectory [7]. The force balance equation typically reads as

$$m_p \frac{d\mathbf{v}}{dt} = \mathbf{F}_D + \mathbf{F}_{SL} + \mathbf{g}V_p[\rho_p - \rho_f] \quad (1)$$

where m_p , V_p , ρ_p are the mass, the volume and the density, respectively, of the particle, ρ_f is the fluid density, and \mathbf{v} , \mathbf{F}_D , \mathbf{F}_{SL} , \mathbf{g} are the corresponding coefficient (column) matrices of the particle velocity \mathbf{v} , the drag force \mathbf{F}_D , the shear lift force \mathbf{F}_{SL} , and the gravity acceleration \mathbf{g} , respectively. Similarly to the study of [7], in the present study the particle dimensions have a scale of micrometres and the relative velocity (or the slip velocity) between the particle and the fluid is very small, resulting in a Stokes flow around the particle. Therefore, the profile lift force, the lift force due to the relative particle rotation with respect to the fluid, the Brownian motion force, the pressure gradient force, the added mass, and the Basset history force are neglected.

Let us first recall the model of drag force acting on a prolate spheroidal particle (or axisymmetric ellipsoidal particle) derived

by Brenner [5] for the case of Stokes flow:

$$\mathbf{F}_D = \pi a \rho_f \nu \mathbf{K} [\mathbf{u} - \mathbf{v}] =: \mathbf{D} [\mathbf{u} - \mathbf{v}] \quad (2)$$

where a is the semi-minor axis of the prolate spheroidal particle with aspect ratio $\lambda = b/a$ (where b is the semi-major axis), ν is the kinematic viscosity of the fluid, and \mathbf{u} , $[\mathbf{u} - \mathbf{v}]$, \mathbf{F}_D , \mathbf{K} , \mathbf{D} are the corresponding coefficient matrices of the fluid velocity \mathbf{u} , the slip velocity $[\mathbf{u} - \mathbf{v}]$, the drag force \mathbf{F}_D , the geometric resistance tensor \mathbf{K} , and the physical resistance tensor \mathbf{D} , respectively. \mathbf{K} is initially defined in the particle frame of reference and is then transformed into the inertial frame of reference. The spherical particle limit renders $\mathbf{K} = 6\mathbf{I}$, where \mathbf{I} is the identity matrix. In the case of prolate spheroidal particles, $\mathbf{D} = \pi a \rho_f \nu \mathbf{K}$ and the calculation of \mathbf{K} in terms of the particle geometry can be found in [7].

The shear-induced lift force acting on a particle arises from the inertia effects in the viscous flow around the particle [11] and the non-uniform slip velocity distribution over the particle and the resulting non-uniform pressure distribution [30]. The celebrated Saffman lift for a freely rotating spherical particle moving at a constant velocity in a linear shear flow $\mathbf{u} = [u_x(z), 0, 0]$ in the $x - z$ plane (whereby $u_{x,z} = \partial u_x / \partial z$ is constant) at low Reynolds number [26,27] reads:

$$\mathbf{F}_{SL} = 6.46 \rho_f a^2 \sqrt{\nu} \operatorname{sgn}(u_{x,z}) |u_{x,z}|^{1/2} \mathbf{B} [\mathbf{u} - \mathbf{v}] \quad (3)$$

with

$$\mathbf{B} = \begin{bmatrix} 0 & 0 & 0 \\ 0 & 0 & 0 \\ 1 & 0 & 0 \end{bmatrix}, \quad (4)$$

where \mathbf{F}_{SL} is the corresponding coefficient (column) matrix of the shear-induced lift force \mathbf{F}_{SL} , and $\operatorname{sgn}()$ is the signum function that extracts the sign of a real number. For linear shear flow $\mathbf{u} = [u_x(z), 0, 0]$ in the x -direction, thus by applying the coefficient matrix \mathbf{B} the Saffman lift force points in the z -direction.

Crowe et al. [6] extended the expression of the Saffman lift, Eq. (3), to the case of a sphere in an arbitrary linear shear flow, expressed here in tensor (vector) notation as

$$\mathbf{F}_{SL} = 6.46 \rho_f a^2 \sqrt{\nu} \frac{1}{\sqrt{|\mathbf{w}|}} [[\mathbf{u} - \mathbf{v}] \times \mathbf{w}], \quad (5)$$

where $\mathbf{w} := \operatorname{curl} \mathbf{u}$ is the fluid vorticity (curl of the fluid velocity) at the particle location. In a linear shear flow $\mathbf{u} = [u_x(z), 0, 0]$, Eq. (5) degenerates to Eq. (3).

Let us analyse the Crowe expression in more detail. Note that the corresponding coefficient (column) matrix of the cross product $[\mathbf{u} - \mathbf{v}] \times \mathbf{w}$ is equal to

$$-2 \mathbf{G}^{skw} [\mathbf{u} - \mathbf{v}],$$

where \mathbf{G}^{skw} is the corresponding coefficient matrix of the spin tensor \mathbf{G}^{skw} (i.e. the skew part of the velocity gradient tensor \mathbf{G}). The magnitude of \mathbf{G}^{skw} can be defined as [31]

$$\|\mathbf{G}^{skw}\| =: \sqrt{2 \mathbf{G}^{skw} : \mathbf{G}^{skw}}.$$

By using the above definition, the spin tensor and the vorticity have the same magnitude, i.e.

$$\|\mathbf{G}^{skw}\| = |\mathbf{w}|,$$

where \mathbf{w} is the coefficient (column) matrix of the fluid vorticity \mathbf{w} at the particle location.

Therefore, the generalised Saffman lift acting on a sphere proposed by Crowe et al. [6] can alternatively be expressed in a matrix notation as

$$\mathbf{F}_{SL} = 6.46 \rho_f a^2 \sqrt{\nu} \frac{1}{\sqrt{\|\mathbf{G}^{skw}\|}} [-2 \mathbf{G}^{skw} [\mathbf{u} - \mathbf{v}]] \quad (6)$$

$$\propto \mathbf{D} \mathbf{G}^{skw} \mathbf{D} [\mathbf{u} - \mathbf{v}], \quad (7)$$

where, in the case of spherical particles, $\mathbf{D} = \pi a \rho_f \nu \mathbf{K} = 6\pi a \rho_f \nu \mathbf{I}$.

The extension of Saffman's model from the spherical particle to an arbitrarily shaped three-dimensional (3D) rigid body moving in a linear shear flow $\mathbf{u} = [u_x(z), 0, 0]$ in the $x - z$ plane (whereby $u_{x,z} = \partial u_x / \partial z$ is constant) was proposed by Harper and Chang [14] and is given by

$$\mathbf{F}_{SL} = \frac{1}{\rho_f \nu^{3/2}} \operatorname{sgn}(u_{x,z}) |u_{x,z}|^{1/2} \mathbf{D} \mathbf{L}_{xz} \mathbf{D} [\mathbf{u} - \mathbf{v}] \quad (8)$$

$$\propto \mathbf{D} \mathbf{L}_{xz} \mathbf{D} [\mathbf{u} - \mathbf{v}], \quad (9)$$

where the coefficient matrix of the lift tensor \mathbf{L}_{xz} was calculated via asymptotic methods and is expressed as

$$\mathbf{L}_{xz} = \begin{bmatrix} A & 0 & B \\ 0 & C & 0 \\ D & 0 & E \end{bmatrix}, \quad (10)$$

where the coefficients of \mathbf{L}_{xz} are given as

$$A = 0.0501, B = 0.0329, C = 0.0373, D = 0.0182, E = 0.0173. \quad (11)$$

Recall that \mathbf{D} reads in the case of prolate spheroidal particles as $\mathbf{D} = \pi a \rho_f \nu \mathbf{K}$ (Eq. (2)), thus one can rewrite Eq. (8) as [11]

$$\mathbf{F}_{SL} = \pi^2 \rho_f a^2 \sqrt{\nu} \operatorname{sgn}(u_{x,z}) |u_{x,z}|^{1/2} \mathbf{K} \mathbf{L}_{xz} \mathbf{K} [\mathbf{u} - \mathbf{v}]. \quad (12)$$

From the above listed studies general model properties could be deduced, namely that all shear-induced lift force models are directly related to the velocity gradient tensor. The gradient tensor has intrinsic properties and can be decomposed into the spin tensor \mathbf{G}^{skw} and the rate of deformation tensor \mathbf{G}^{sym} (i.e. the symmetric part of \mathbf{G}), whereby the symmetric part can be further decomposed into its volumetric and deviatoric parts, i.e. $\mathbf{G}^{sym} = \mathbf{G}^{sym.vol} + \mathbf{G}^{sym.dev}$. In the case of incompressible flows, $\mathbf{G}^{sym.vol} = \mathbf{0}$.

As illustrated in Eq. (7), the lift model proposed by Crowe et al. [6] can be written as a force proportional to the skew part of the velocity gradient tensor times slip velocity. Note that the lift tensor \mathbf{L}_{xz} of [14] is neither skew nor symmetric, and can be interpreted as a weighted sum of various contributions. Applying the described rationale, the Harper & Chang's lift model can also be written as a sum of the force proportional to the skew part (contributed by the coefficient D of the lift tensor), the symmetric part of velocity gradient tensor (contributed by the coefficient B) and the inertia effect of the Stokes drag (contributed by the coefficients A , C and E) times the slip velocity. Therefore, a generalised form of the shear-induced lift force model can be expressed as

$$\mathbf{F}_{SL} = \mathbf{D} [\mathbf{C}_0 + c_1 \mathbf{G}^{skw} + c_2 \mathbf{G}^{sym.vol} + c_3 \mathbf{G}^{sym.dev}] \mathbf{D} [\mathbf{u} - \mathbf{v}], \quad (13)$$

where \mathbf{C}_0 is a fluid-property-related coefficient matrix, c_1 , c_2 and c_3 are fluid-property-related coefficients, $\mathbf{G}^{sym.vol}$ and $\mathbf{G}^{sym.dev}$ are the coefficient matrices of volumetric and deviatoric parts, respectively, of the rate of deformation tensor \mathbf{G}^{sym} . The term $\mathbf{D} \mathbf{C}_0 \mathbf{D} [\mathbf{u} - \mathbf{v}]$ has the effect of changing the shape of the Stokes orbit [14], and represents the inertial effect of the Stokes drag [7]. The general form of the shear induced lift force model can now serve as the basis for the derivation of a unified lift force model, based on the established lift force models, which would preserve the effects of the streamwise and non-streamwise flow shear effects, but would computationally be less demanding than alternative models [7,9].

In fluid flows that are dominated by the streamwise flow shear (e.g. Poiseuille flow) or in the case of spherical particles moving in an arbitrary non-uniform flow (e.g. lid-driven cavity flow), our previous studies [7,9] have shown that the coefficients B , C and E of the lift tensor (Eq. (10)) proposed by Harper and Chang [14] have insignificant influence on the shear-induced lift force on the particle. The coefficient A of the lift tensor generates a lift

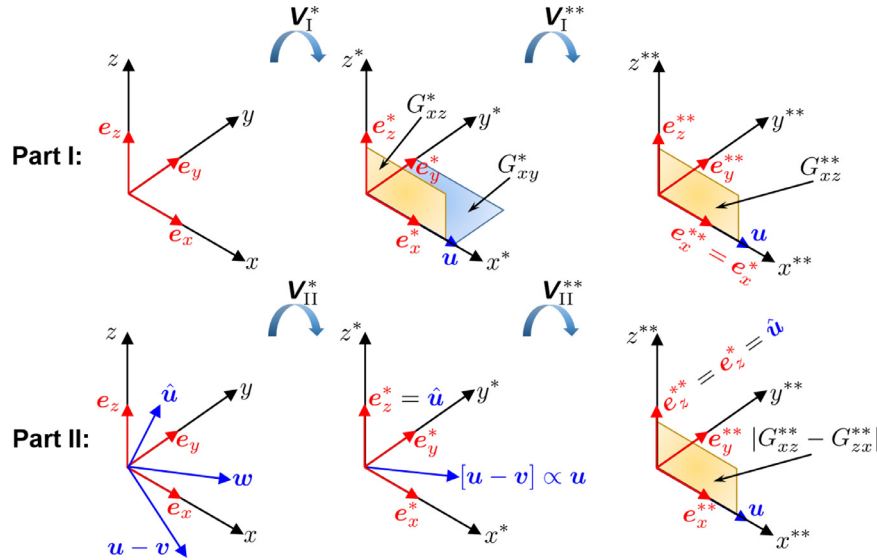


Fig. 1. Illustration of two coordinate rotations of two different shear-induced lift models for prolate spheroidal particles; Part I: Cui et al., *Int. J. Multiph. Flow*, 2018 [7]; Part II: Cui et al., *Int. J. Multiph. Flow*, 2019 [9].

component acting in the same direction as the drag force, and represents the inertia effect of the drag, which is much smaller than the drag itself. The main contribution to the lift component in the direction perpendicular to the drag force is given by the coefficient D of the lift tensor, which is only related to the skew part of the velocity gradient tensor. Based on the previous arguments it is reasonable to simplify the lift tensor of [14] by taking into account only the coefficients A and D . Note that the lift component produced by the coefficient A arises from the velocity difference in the direction of the drag force. By assuming that the particle slip velocity is parallel to the fluid velocity along the particle trajectory (assumption used by Saffman et al. [26] and Cui et al. [9]), it follows that $\mathbf{C}_0 = c_0 \mathbf{I}$, where c_0 is a fluid-property-related coefficient. Under such a condition, Eq. (13) can be simplified to

$$\mathbf{F}_{SL} = \mathbf{D} [c_0 \mathbf{I} + c_1 \mathbf{G}^{skw}] \mathbf{D} [\mathbf{u} - \mathbf{v}]. \quad (14)$$

As Eq. (14) must also be valid for spherical particles, c_0 and c_1 can be calculated by comparing Eq. (14) with Eqs. (6) and (12) (i.e. analogy arguments), resulting in

$$c_0 = \frac{A \sqrt{\|\mathbf{G}^{skw}\|}}{\rho_f \nu^{3/2}} \quad \text{and} \quad c_1 = \frac{-2D}{\rho_f \nu^{3/2} \sqrt{\|\mathbf{G}^{skw}\|}}. \quad (15)$$

Although the lift model of [6] is only valid for spherical particles, it can also be used to establish a lift model for non-spherical particles via analogy arguments, as the lift model of [6] is a generalisation of the Saffman lift model, which can easily be deduced from the coefficient D of the lift tensor [14], i.e. $36\pi^2 D = 6.46$.

By inserting Eq. (15) into Eq. (14), the simplified unified shear-induced lift force model for prolate spheroidal particles can finally be expressed as:

$$\mathbf{F}_{SL} = \pi^2 \rho_f a^2 \sqrt{\nu} \frac{1}{\sqrt{\|\mathbf{G}^{skw}\|}} \mathbf{K} [A \|\mathbf{G}^{skw}\| \mathbf{I} - 2D \mathbf{G}^{skw}] \mathbf{K} [\mathbf{u} - \mathbf{v}]. \quad (16)$$

In the case of spherical particles, $\mathbf{K} = 6\mathbf{I}$, so that the lift component calculated by the second part of the present model (i.e. $c_1 \mathbf{G}^{skw}$) is identical to the lift model of [6].

2.1. Differences between the shear-induced lift model of Part I, Part II, and the present model

At first, we give a short description of the formulation of the shear-induced lift model of Part I and II. As aforementioned, Part I calculates the shear-induced lift force arising from the dominate streamwise flow shear, whereas Part II takes the non-streamwise flow shear into account. Both models are derived by means of two coordinate rotations.

In Part I, as shown in Fig. 1, the first coordinate rotation, described by the rotation matrix \mathbf{V}_I^* , rotates the inertial frame with base vectors \mathbf{e}_i ($i = 1, 2, 3$) into a new reference frame with base vectors \mathbf{e}_i^* ($i = x, y, z$), so that the \mathbf{e}_x^* is parallel to the streamwise direction at the particle location. As only the lift force due to the streamwise flow shear is included in the analysis, for the flow velocity at the coordinate system \mathbf{e}_i^* , only two shear rates of $G_{xy}^* = \partial u_x^* / \partial y^*$ and $G_{xz}^* = \partial u_x^* / \partial z^*$ remain to be taken into account. The second coordinate rotation by the rotation matrix \mathbf{V}_I^{**} is a rotation around the x^* -axis. The goal of the rotation is to compress the two streamwise shear rates in the coordinate system \mathbf{e}_i^* , i.e. G_{xy}^* and G_{xz}^* , into one shear rate G_{xz}^{**} in the new reference frame with base vectors \mathbf{e}_i^{**} ($i = x, y, z$). \mathbf{G}^{**} can be calculated by $\mathbf{G}^{**} = \mathbf{V}_I^{**T} \mathbf{V}_I^* \mathbf{G} \mathbf{V}_I^* \mathbf{V}_I^{**T}$. Next, to be able to apply the single linear shear flow model [14] in a more general case, the following form was proposed in Part I:

$$\mathbf{F}_{SL,I} = \pi^2 \rho_f a^2 \sqrt{\nu} \sqrt{|G_{xz}^{**}|} \mathbf{V}_I^{**T} \mathbf{V}_I^{*T} \mathbf{K}^{**} \mathbf{L}_{xz}^{**} \mathbf{K}^{**} \mathbf{V}_I^{**} \mathbf{V}_I^* [\mathbf{u} - \mathbf{v}], \quad (17)$$

where $\mathbf{K}^{**} = \mathbf{V}_I^{**T} \mathbf{V}_I^* \mathbf{K} \mathbf{V}_I^* \mathbf{V}_I^{**T}$, and \mathbf{L}_{xz}^{**} is the corresponding coefficient matrix of the lift tensor \mathbf{L}_{xz} in the coordinate system \mathbf{e}_i^{**} .

Formal studies [2,3,6,30] show that the shear-induced lift force is in the direction of the cross product between the particle slip velocity (i.e. $[\mathbf{u} - \mathbf{v}]$) and the vorticity (i.e. \mathbf{w}) at the particle location. The unit direction of the shear-induced lift force is defined in vector notation as $\hat{\mathbf{u}} = [\mathbf{u} - \mathbf{v}] \times \mathbf{w} / \|\mathbf{u} - \mathbf{v}\| \times \mathbf{w}$.

In Part II, as illustrated in Fig. 1, the first step is the determination of the rotation matrix \mathbf{V}_{II}^* , aligning the unit direction vector $\hat{\mathbf{u}}$ with the base vector \mathbf{e}_z^* in the reference frame with base vectors \mathbf{e}_i^* ($i = x, y, z$). Note that $\hat{\mathbf{u}}$ is the unit vector of the cross product between the particle slip velocity and the vorticity. In other words, $\hat{\mathbf{u}}$ is perpendicular to the plane spanned by vectors $[\mathbf{u} - \mathbf{v}]$ and \mathbf{w} . Therefore, in the coordinate system \mathbf{e}_i^* , $[\mathbf{u} - \mathbf{v}]$ lies in the $x^* - y^*$ plane and the z^* -component of $[\mathbf{u} - \mathbf{v}]$ is zero.

Table 1

The comparison of three shear-induced lift models for prolate spheroidal particles.

| | Part I [7] | Part II [9] | Present model |
|--|------------|-------------|---------------|
| Applicability in streamwise flow shear | Yes | Yes | Yes |
| Applicability in non-streamwise flow shear | No | Yes | Yes |
| Accuracy in streamwise flow shear | High | Medium | Medium |
| Accuracy in non-streamwise flow shear | N/A. | Medium | Low |
| Computational cost | High | High | Low |

In the following we make a critical assumption: *the particle slip velocity is parallel to the fluid velocity*, i.e. $[\mathbf{u} - \mathbf{v}] \propto \mathbf{u}$ or $\mathbf{v} \propto \mathbf{u}$. In fact, this assumption is one of the key assumptions of Saffman lift [26,27,32]. If the particle size is in the micro and submicron range, this assumption is usually satisfied since gravity plays only a minor role with respect to other forces acting on the particle. Under such a condition, the fluid velocity in the coordinate system \mathbf{e}_i^* lies in the $x^* - y^*$ plane with its z^* -component being zero, i.e. $\mathbf{u}^* = \mathbf{V}_{\parallel}^* \mathbf{u} = [u_x^*, u_y^*, 0]^T$, where \mathbf{u}^* and \mathbf{u} are the corresponding coefficient (column) matrices of fluid velocities in the coordinate systems \mathbf{e}_i^* and \mathbf{e}_i , respectively. The second coordinate rotation by the rotation matrix $\mathbf{V}_{\parallel}^{**}$ rotates the coordinate system \mathbf{e}_i^* around the z^* -axis into a new coordinate system \mathbf{e}_i^{**} , so that the fluid velocity in the new coordinate system \mathbf{e}_i^{**} is in the direction of \mathbf{e}_x^{**} . After two coordinate rotations, in the coordinate system \mathbf{e}_i^{**} , the particle can be considered as moving in a linear shear flow $\mathbf{u}^{**} = \mathbf{V}_{\parallel}^{**} \mathbf{u}^* = [u_x^{**}, 0, 0]^T$ in the $x^{**} - z^{**}$ plane, with the corresponding shear rate being $|C_{xz}^{**} - G_{zx}^{**}|$. Therefore, in the coordinate system \mathbf{e}_i^{**} , the shear lift force can be calculated by using lift models which are devised for linear shear flows. The novel shear lift force for prolate spheroidal particles is expressed as

$$\mathbf{F}_{\text{SL,II}} = \pi^2 \rho_f a^2 \sqrt{v} \sqrt{|G_{xz}^{**} - G_{zx}^{**}|} \mathbf{V}_{\parallel}^{*T} \mathbf{V}_{\parallel}^{**T} \mathbf{K}^{**} \mathbf{L}^{**} \mathbf{K}^{**} \mathbf{V}_{\parallel}^* \mathbf{V}_{\parallel}^* [\mathbf{u} - \mathbf{v}]. \quad (18)$$

In fluid flows which are dominated by the streamwise flow shear, the present model has the same accuracy as the lift force model of Part II since the assumption is the same (i.e. the particle slip velocity is parallel to the fluid velocity), and is less accurate than the lift force model of Part I [7]. In fluid flows in which the non-streamwise flow shear also plays an important role, the present model is less accurate than the lift model of Part II [9] in the case of non-spherical particles since the coefficients B , C and E of the lift tensor [14] were not taken into account. Table 1 summarises the limitations and advantages of the three different shear-induced lift models for prolate spheroidal particles. In Section 3.2, a quantitative study on the accuracy of the computational results by using the proposed unified shear lift force model is performed.

It should be noted that the lift tensor proposed by [14] is applicable for any arbitrarily shaped 3D body. Therefore, the present model can also be used to compute the shear-induced lift force on oblate particles or other shaped particles, by replacing the (geometric) resistance tensor \mathbf{K} for prolate spheroids with corresponding (geometric) resistance tensors for oblate particles.

The computational cost of the present model was measured by using the profiling function of MATLAB®. The results show that the present model is about 68 times faster than the lift model of Part I and Part II, which is not a surprise, as both previous models use two additional coordinate system transformations in order to calculate the shear lift force components.

The numerical algorithms used in computation of the kinematics, the dynamics of translational motion, and the dynamics of rotational motion of prolate spheroidal particles are summarised in [7], and will thus not be repeated here. The particle tracking algorithms have been implemented into MATLAB® and OpenFOAM®, which were used in the computational studies of the

numerical verification of the unified shear lift force model. The implicit Euler backward scheme was applied in both codes. The fluid flow solver within the OpenFOAM® distribution used is the icoFoam, which solves the incompressible laminar Navier-Stokes equations using the PISO algorithm.

3. Numerical verification of the novel shear-induced lift force model for prolate spheroidal particles in poiseuille and lid-driven cavity flows

Direct validation of the present model by comparing it with direct numerical simulation (DNS) results of a fully-resolved prolate spheroidal particle or experiments is difficult. The difficulty lies in the fact that, from both the experimental measurement and the DNS point of view, the results of simulated or measured fluid dynamic forces are in the form of only one single fluid force. Unfortunately, with the results of an interface resolved simulation there still remains the problem of evaluating each single fluid force contribution, such as the drag, the Magnus lift, the profile lift, the lift due to viscous force (i.e. Saffman-type lift) and the lift due to non-uniform pressure distribution around the particle. In most recent studies [1,24,28,37], where the particle is fully-resolved, only the profile lift of a stationary non-spherical particle in an uniform flow was calculated by varying the angle of incidence and the Reynolds number. The profile lift is, in fact, a component of the drag force, which is described by a tensorial drag coefficient for non-spherical particles [29]. To the best of our knowledge, only Hölzer and Sommerfeld [15] provides the DNS data for the shear-induced lift force acting on a prolate spheroid by performing lattice Boltzmann (LB) simulations. However, as mentioned by [15], the shear-induced lift on a prolate spheroid is very sensitive to the size of the fluid domain, hence a good agreement with Saffman lift can hardly be obtained.

Although a direct validation is difficult, the present lift model can be validated indirectly by comparing it with the lift model of Part II. The lift model of Part II improved the lift model of Harper & Chang by only performing coordinate system rotations, which is physically correct for every numerical step if the assumptions hold exactly. Harper & Chang's model has been validated by experimental data in their paper and is widely applied in numerous publications. From this point of view, we adopt the Harper & Chang's model as an established one and considered it as a reference result. Also, in [7], the lift model of Part II has been verified by comparing it with DNS results of a sphere and LB simulation results for a prolate spheroid in Couette flow given by Hölzer and Sommerfeld [15], and a good agreement has been found. In this work, the present model is numerically verified by comparing it with Part I, Part II and two other lift models in Poiseuille and lid-driven cavity flows.

3.1. Poiseuille flow

The novel shear-induced lift force model (Eq. (16)) is first verified in a Poiseuille pipe flow, which is dominated by the streamwise flow shear. As shown in Fig. 2, the complete simulation setup is the same as that used in [7,9]. The pipe radius R is

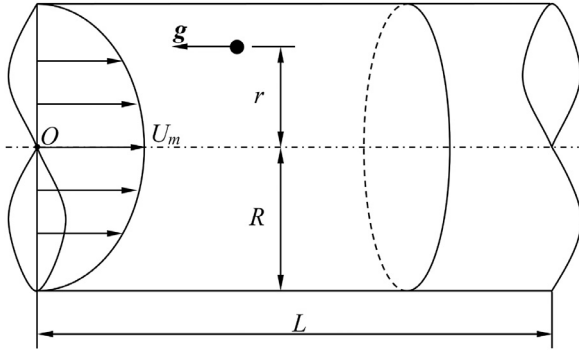


Fig. 2. Schematic diagram of a particle in Poiseuille flow.

Table 2

Information of two initial positions P_1 and P_2 of the particle in Poiseuille flow.

| Point | Position | Euler Angle | Flow Direction |
|-------|-------------------------------|-----------------------|-------------------------------------|
| P_1 | $[0, -r, 0]^T$ | $[0, \pi/2, 0]^T$ | $[0.5U_m, 0, 0]^T$ |
| P_2 | $[0.6124r, -0.6124r, 0.5r]^T$ | $[\pi/4, \pi/3, 0]^T$ | $[U_m/\sqrt{2}, U_m/\sqrt{2}, 0]^T$ |

2.1 mm. The fluid density is 1000 kg/m^3 and the fluid kinematic viscosity is $1 \text{ mm}^2/\text{s}$. The flow field of the Poiseuille pipe flow is analytically given in cylindrical coordinates by

$$u = U_m \left[1 - \left[\frac{r}{R} \right]^2 \right] \quad (19)$$

where r is the radial distance between the particle and the pipe centreline, and U_m is the maximum flow velocity at $r = 0$ with a magnitude of 0.5 m/s being used in the present study. The gravity acceleration \mathbf{g} acts in the opposite streamwise direction.

In the simulation of Poiseuille flow, only one particle is placed in the flow field, and its semi-major axis b points into the pipe centreline. The volume equivalent diameter of the particle D_p is $20 \mu\text{m}$, and the particle density ρ_p is 2560 kg/m^3 . The initial radial distance between the particle and the pipe centreline r is 0.1 mm . The initial particle velocity is $\mathbf{v} = 0.99\mathbf{u}$, therefore the particle Reynolds number at the start of simulation is $Re_p = U_m R / \nu \approx 0.1$. In the present study, the particle is a Lagrangian point particle and therefore the Segré-Silberberg effect was ignored. The particle will move to the pipe centreline due to the action of the shear-induced lift force. Moreover, regardless of the initial circumferential location of the particle, at the same radial distance r , the particle must experience the same magnitude of the lift force, which has to act radially towards the pipe centreline. In order to validate this ability of the present model on capturing the correct direction and magnitude of the lift force regardless of the initial particle positions, the initial circumferential location of the particle as well as the flow direction were varied. The informations on the two initial positions of the particle being used in the present study (i.e. P_1 and P_2) are summarised in Table 2. The radial distances between the particle and the pipe centreline at P_1 and P_2 are identical. The orientation of the particle is controlled by the Euler angle or Euler parameters [7], listed in Table 2, and the semi-major axis b of the particle for both initial positions points towards the pipe centreline.

The present shear lift model (Eq. (16)) is compared with lift models proposed by Crowe et al. [6] (Eq. (5)) for the case of spherical particles, and those of Part I and Part II for the non-spherical case. The corresponding numerical algorithms for calculating the shear-induced lift forces of Part I and II, which use the lift tensor of [14] as a basis, are given in [7,9]. Among these shear-induced lift models, the lift force model proposed by Part I [7] is considered as the benchmark model, since it is identical to the lift force

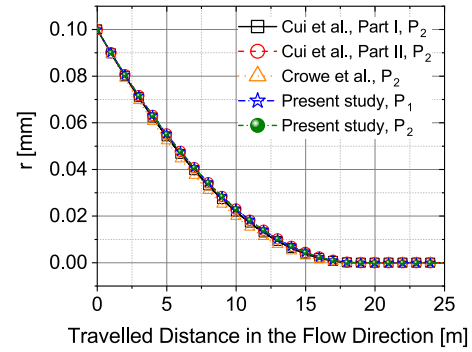


Fig. 3. Translational motion of a spherical particle in Poiseuille flow for different shear lift force models and initial positions (tracking time: 50 s, time step: $10 \mu\text{s}$, $D_p = 20 \mu\text{m}$).

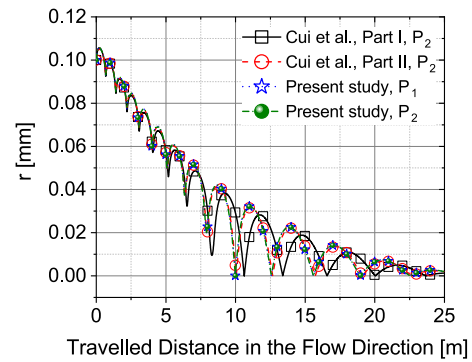


Fig. 4. Translational motion of a prolate spheroidal particle in Poiseuille flow for different initial positions and aspect ratios (tracking time: 50 s, time step: $10 \mu\text{s}$, $\lambda = 10$, $D_p = 20 \mu\text{m}$).

model of [14] in the case of the linear shear flow and produces the same computational results for P_1 and P_2 . The lift force model of [6] only computes the lift component perpendicular to the slip velocity for spherical particles; and the lift force model of Part II is slightly less accurate than the model of Part I for the reason that the underlying assumption of "the particle slip velocity is parallel to the fluid velocity along the particle trajectory" is not perfectly satisfied along the computed particle trajectory.

As shown in Fig. 3, in the case of spherical particles, the difference in results between the present model and the benchmark model is very small, and shows an excellent agreement with the lift model of Part II. In the case of prolate spheroidal particles, the numerical discrepancy between the present model and the benchmark model steadily increases but is still acceptable as highlighted in Fig. 4. The difference in results between the present model and the lift model of Part II shows a good agreement as well. This is reasonable since in fluid flows dominated by the streamwise flow shear the coefficients A and D play the most important roles in calculating the lift force, which agrees with the finding in [9]. Moreover, it is shown that the numerical results for the two different initial particle positions, i.e. P_1 and P_2 , are identical, proving the validity of the present model for calculating the shear-induced lift force in arbitrary non-uniform flows which are dominated by the streamwise flow shear.

Fig. 5 plots the ratio between the lift components calculated by the present model and the lift model of Part I. In the streamwise direction (i.e. x -direction), the lift component calculated by the present model (i.e. $F_{SL,x,present}$) is slightly larger than the lift component calculated by the lift model of Part I (i.e. $F_{SL,x,part}$). However,

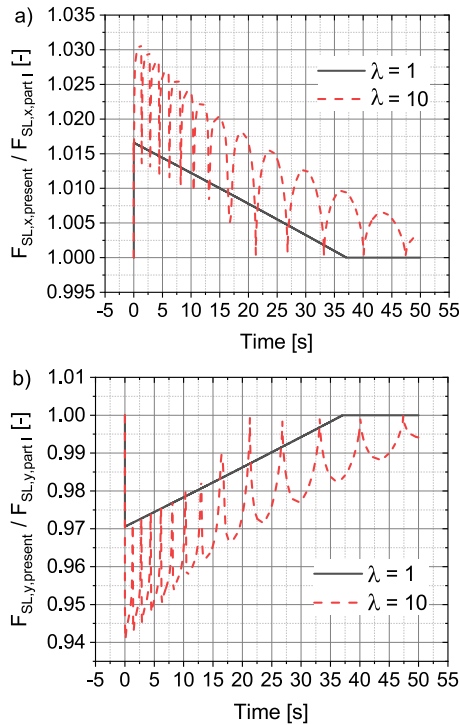


Fig. 5. Time evolution of the ratio of the lift force calculated by the present model to the lift force calculated by the model of Part I of a particle moving in Poiseuille flow for different aspect ratios; a) the ratio of lift forces in the streamwise direction calculated by two lift models; b) the ratio of lift forces in the radial direction calculated by two lift models (initial particle position: P_1 , tracking time: 50 s, time step: $10 \mu\text{s}$, $D_p = 20 \mu\text{m}$).

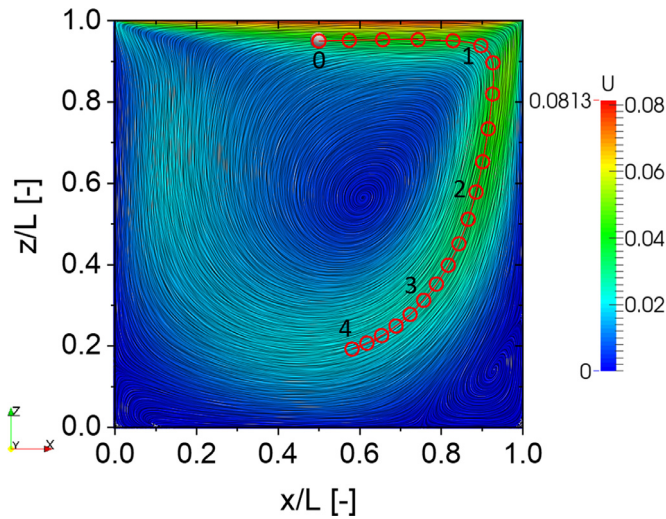


Fig. 6. Numerically computed flow streamlines of a 3D lid-driven cavity flow in a cube, slice at $y = 0.4L$ ($Re = 470$, the dimension of the domain: $L = 0.1\text{m}$, the top wall moves in the x -direction).

in the direction perpendicular to the streamwise direction (i.e. y -direction), this ratio is slightly smaller than one. In the case of spherical particles, the difference between the two models originates in how accurate the assumption of “the particle slip velocity is parallel to the fluid velocity along the particle trajectory” can be satisfied. In the case of prolate spheroidal particles, in addition to satisfying the assumption, the absence of the coefficients B , C and E of the lift tensor in constructing the present model also contribute to the increases in the difference of the results.

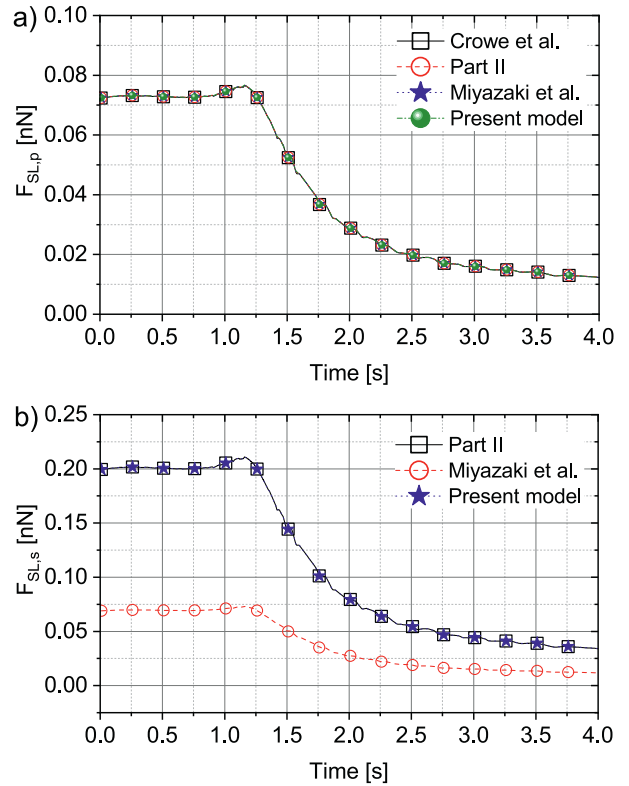


Fig. 7. Time evolution of the lift force components of a spherical particle moving in the lid-driven cavity flow for different shear-induced lift force models; a) lift component in the direction perpendicular to the slip velocity; b) lift component in the direction of the slip velocity (tracking time: 4 s, time step: $10 \mu\text{s}$, $D_p = 100 \mu\text{m}$).

3.2. Lid-driven cavity flow

The lid-driven cavity flow is an ideal test case since the non-streamwise flow shear also plays an important role on calculating the shear-induced lift force [8,9,35]. In the present study, the complete set-up of the simulation is the same as being used by Tsorng et al. [35] (i.e. for the fluid phase) and Cui et al. [9] (i.e. for the particle phase). The cavity is a cubic domain with the edge length L equal to 0.1m . The density and the kinematic viscosity of the fluid are 1210kg/m^3 and $17.3\text{mm}^2/\text{s}$, respectively. The upper wall moves with the constant velocity of $U_0 = 0.0813\text{m/s}$, yielding the flow Reynolds number $Re = U_0 L/\nu = 470$. The boundary conditions on all the walls are the non-slip conditions. Fig. 6 plots the computed flow streamlines. The particle is released at the position of $[0.4L, 0.5L, 0.95L]^T$ with its semi-major axis b pointing in the z -direction. The initial particle velocity is equal to the flow velocity at the particle location. The particle volume equivalent diameter D_p is $100 \mu\text{m}$, and the particle density is 2560kg/m^3 . In the present study, the considered fluid forces acting on the particle are the Brenner’s drag [5] and the shear-induced lift force calculated by several different shear-induced lift force models, i.e. lift models proposed by Miyazaki et al. [23], Crowe et al. [6], Cui et al. [9] and the present model.

In order to have a clear set-up for the evaluation of the difference in the results between the applied shear lift models, the first comparison is based on the trajectory of a spherical particle moving in a lid-driven cavity flow, under the action of the Brenner’s drag and the gravity reduced by buoyancy, as presented in Fig. 6. The flow field has been computed in [8]. The simulation time for particle tracking is 4 s, and the numbers along the particle trajectory indicate the particle locations at corresponding times.

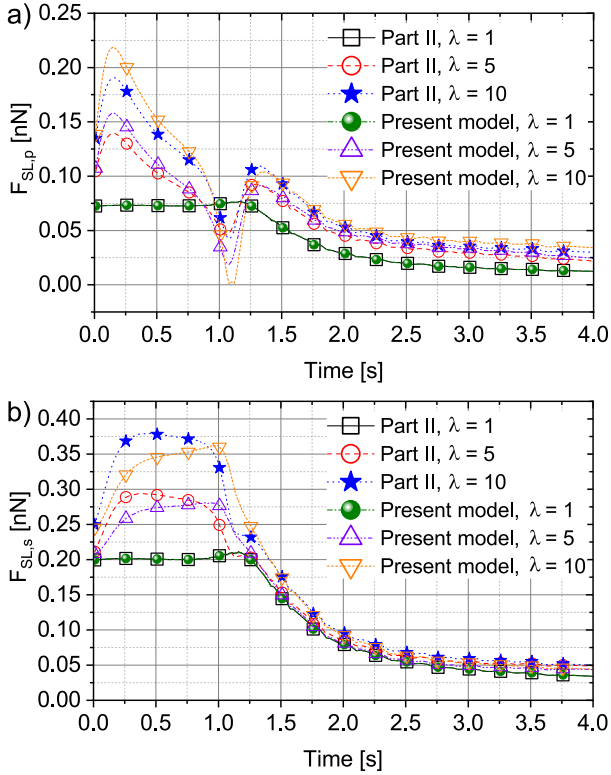


Fig. 8. Time evolution of the lift force components of a prolate spheroidal particle moving in the lid-driven cavity flow for different shear-induced lift force models and aspect ratios; a) lift force component in the direction perpendicular to the slip velocity; b) lift force component in the direction of the slip velocity (tracking time: 4 s, time step: $10 \mu\text{s}$, $D_p = 100 \mu\text{m}$).

The lift force acting on a particle is calculated along the particle trajectory, but is not taken into account when computing the trajectory, so in this way the particle trajectories are identical for all the cases which allows us to study the differences in lift force evaluations between the selected lift force models.

As aforementioned, the lift tensor [14] in Eq. (8) not only produces the lift force component in the direction perpendicular to the drag force, i.e. $[\mathbf{u} - \mathbf{v}] \times \mathbf{w}$, but also yields a lift force component in the direction of the drag, i.e. $[\mathbf{u} - \mathbf{v}]$. Therefore, the comparison of different lift force models requires separation of the lift force (i.e. \mathbf{F}_{SL}) into a component in the direction of the slip velocity (i.e. $\mathbf{F}_{SL,s}$) and into a component perpendicular to the slip velocity (i.e. $\mathbf{F}_{SL,p}$). The magnitudes of $\mathbf{F}_{SL,s}$ and $\mathbf{F}_{SL,p}$ are calculated as:

$$F_{SL,s} = \frac{\mathbf{F}_{SL} \cdot [\mathbf{u} - \mathbf{v}]}{|\mathbf{u} - \mathbf{v}|} \quad \text{and} \quad F_{SL,p} = \sqrt{|\mathbf{F}_{SL}|^2 - F_{SL,s}^2} \quad (20)$$

In the case of spherical particles, the lift coefficient arising from $F_{SL,p}$ is identical to the Saffman-lift coefficient. In the case of non-spherical particles, it's difficult to define the lift coefficient since the cross-sectional area of the particle perpendicular to the direction of the slip velocity varies due to the changing relative orientation.

The computational results of the lift force components $F_{SL,p}$ and $F_{SL,s}$ acting on a spherical particle by using different shear-induced lift force models are plotted in Fig. 7. The results of $F_{SL,p}$ calculated by four different lift force models show excellent agreement. This is expected since the lift force component produced by the second part of the present model (determined by $c_1 \mathbf{G}^{skw}$) is identical to the values of $F_{SL,p}$ calculated by the lift force models of [6], [23] and [9]. As shown in Fig. 7b, the results of $F_{SL,s}$ calculated by the present model and the lift force model of Part II also show

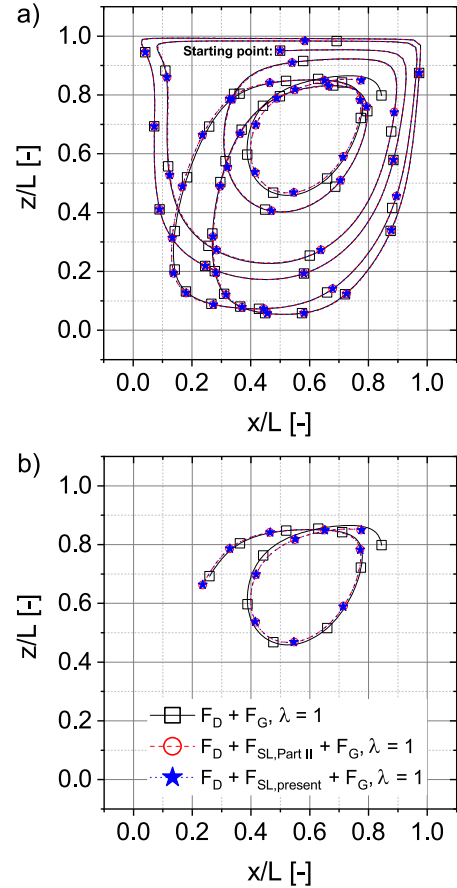


Fig. 9. The translational motion of a spherical particle in the lid-driven cavity flow taking into account the shear-induced lift force; a) time period 0 s – 100 s; b) time period 80 s – 100 s (tracking time: 100 s, time step: $10 \mu\text{s}$, $D_p = 100 \mu\text{m}$).

excellent agreement since the lift force on a sphere calculated by Part II only takes into consideration the coefficients A and D . The lift model of [6] does not calculate the lift force component $F_{SL,s}$. In addition, there exists a numerical discrepancy in the results between the present model and the lift force model of [23]. However, this numerical discrepancy is acceptable since in the case of spherical particles $F_{SL,s}$ acts in the same direction as the drag but is much smaller than the drag, which corresponds to the finding of [32].

In the case of prolate spheroidal particles, the magnitudes of the lift force components of $F_{SL,p}$ and $F_{SL,s}$ both increase with increasing aspect ratios, as shown in Fig. 8. The particle rotates due to the flow resistance and tends to align its primary axis b along the flow direction, where the particle with this orientation angle experiences a minimum drag [9]. However, at this orientation angle the cross-sectional area of the prolate spheroidal particle is the largest in the direction perpendicular to the slip velocity, leading to an increase in the lift force magnitude [9]. Moreover, the numerical discrepancy between the present model and the lift force model of Part II increases with increasing aspect ratios. However, the maximum numerical discrepancy at $\lambda = 10$ is about 13%, and can, therefore, be considered as acceptable. The main reason lies in the absence of the coefficients B , C and E of the lift tensor while constructing the present model.

Finally, the influence of the shear-induced lift force on the particle trajectories for different aspect ratios, Fig. 9 (i.e. spherical particle) and Fig. 10 (i.e. prolate spheroidal particle), is studied. In this final case, simulation results were obtained by including the

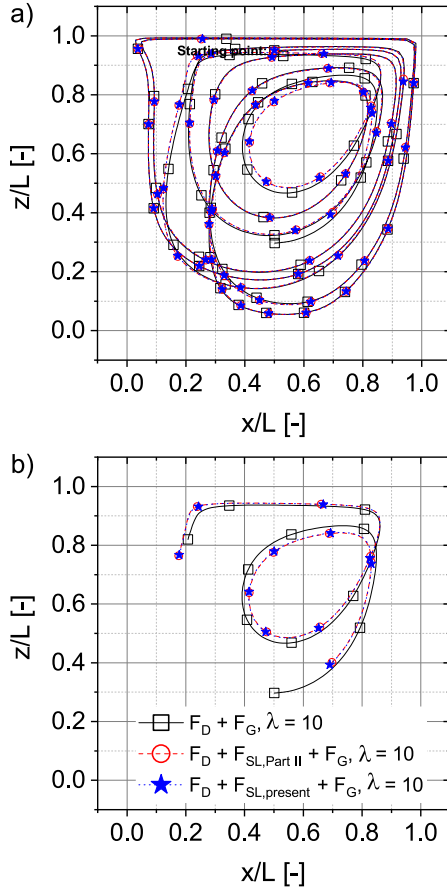


Fig. 10. The translational motion of a prolate spheroidal particle in the lid-driven cavity flow taking into account the shear-induced lift force; a) time period 0 s – 120 s; b) time period 100 s – 120 s (tracking time: 120 s, time step: 5 μ s, $D_p = 100 \mu$ m).

action of the lift force when computing the particle trajectory. The entire simulation time varies between 100 s and 120 s depending on the aspect ratio, and the time intervals between two neighbouring positions are 2 s. Figs. 9a and 10 a plot the entire time range, and Figs. 9b and 10 b shows only the last 20 s in order to emphasize the difference between the computed trajectories. In all cases, the influences of the shear-induced lift force on the particle trajectories are evident, as illustrated in Figs. 9b and 10 b. Fig. 11 plots the lift force components (i.e. $F_{SL,s}$ and $F_{SL,p}$) along the particle trajectory. For the spherical particle (i.e. $\lambda = 1$), $F_{SL,s}$ is proportional to the $F_{SL,p}$, whereas $F_{SL,s}$ becomes disproportional to the $F_{SL,p}$ at an aspect ratio of $\lambda = 10$. The reason is that the lift force model for prolate spheroidal particles of Part II also takes into account the coefficients B , C and E of the lift tensor. However, as illustrated in Fig. 10, the difference between the present model and the lift force model of Part II in the computed particle trajectories is very small, therefore neglecting the coefficients B , C and E by the present model could be justified.

4. Conclusions

The present work proposes a general form of the shear-induced lift force model which can be related to any existing shear-induced lift model. The model divides the lift into four components, arising from the skew part of the velocity gradient tensor (i.e. \mathbf{G}^{skw}), the volumetric and the deviatoric parts of the symmetric part of the velocity gradient tensor, ($\mathbf{G}^{sym, vol}$ and $\mathbf{G}^{sym, dev}$), and the inertial effect of the Stokes drag. In the incompressible flow case,

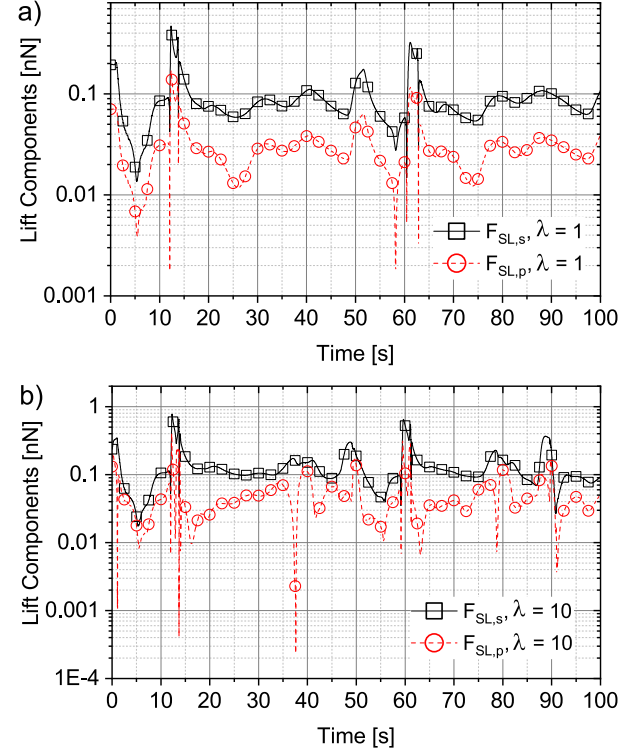


Fig. 11. Time evolution of lift components of a particle moving in lid-driven cavity flow including the action of the lift force on the particle calculated by the present model for different aspect ratios; a) $\lambda = 1$; b) $\lambda = 10$ (tracking time: 100 s, time step: 5 – 10 μ s, $D_p = 100 \mu$ m).

$\mathbf{G}^{sym, dev} = \mathbf{0}$ holds and can therefore be neglected. The novelty of the present work is the derivation of a simplified version of the unified shear-induced lift force model, with the goal of being applicable to the calculation of the lift force acting on a prolate spheroidal particle moving in an arbitrary non-uniform flow. The unified model is derived via analogy arguments and only takes into account the lift force component caused by \mathbf{G}^{skw} (i.e. coefficient D of the lift tensor) and the lift force component caused by the part of the inertial effect of the Stokes drag (i.e. coefficient A of the lift tensor), whereas the coefficients B , C and E of the lift tensor [14] are neglected. The proposed unified lift force model for prolate spheroidal particles can be used in Lagrangian particle tracking and is applicable in flow cases with both streamwise and non-streamwise flow shear and is, in comparison with the lift models of Part I and II, computationally much more efficient.

The unified model is first verified in the Poiseuille flow case by simulating the axial migration of a prolate spheroidal particle at two different points with the same radial coordinates. The computed particle trajectories for two initial particle locations by using the unified model are the same, proving the validity of the unified lift force model for calculating the lift force in arbitrary flows. The difference in the results between the unified lift force model and the lift force model of Part I steadily increases with increasing aspect ratio but remains acceptable, which can be attributed to the assumption of the particle slip velocity being parallel to the fluid velocity along the particle trajectory. In order to verify the ability of the unified lift force model to take into account the non-streamwise flow shear, the present model is compared with several established generalised Saffman-type lift force models in case of the lid-driven cavity flow. In the case of spherical particles, the values of the lift force component perpendicular to the slip velocity calculated by all lift force models are the same. In the case of prolate spheroidal particles, the differences in particle

trajectories calculated by the unified lift force model and the lift force model of Part II is very small, and the corresponding magnitudes of lift forces between two models for the case of $\lambda = 10$ are less than 13%, which is considered to be acceptable. The reason for this difference lies in the absence of the coefficients B , C and E from the lift tensor when constructing the unified lift force model. Finally, compared with the lift models of Part I and II, the computational effort of the unified lift force model is significantly decreased (i.e. 68 times faster than the lift model of Part II) proving the model to be suitable for implementation in Lagrangian tracking of a large amount of particles.

Declarations of Conflict Interest

None.

Acknowledgement

The authors thank the Deutsche Forschungsgemeinschaft for the financial support in the framework of the project STE 544/58.

References

- Andersson HI, Jiang F. Forces and torques on a prolate spheroid: low-Reynolds-number and attack angle effects. *Acta Mech* 2018. doi:10.1007/s00707-018-2325-x.
- Auton TR. The lift force on a spherical body in a rotational flow. *J Fluid Mech* 1987;183(-1):199. doi:10.1017/s002211208700260x.
- Auton TR, Hunt JCR, PrudHomme M. The force exerted on a body in inviscid unsteady non-uniform rotational flow. *J Fluid Mech* 1988;197(-1):241. doi:10.1017/s0022112088003246.
- Bagchi P, Balachandar S. Effect of free rotation on the motion of a solid sphere in linear shear flow at moderate re. *Phys Fluids* 2002;14(8):2719–37. doi:10.1063/1.1487378.
- Brenner H. The stokes resistance of an arbitrary particle. *Chem Eng Sci* 1963;18(1):1–25. doi:10.1016/0009-2509(63)80001-9.
- Crowe CT, Schwarzkopf JD, Sommerfeld M, Tsuji Y. *Multiphase flows with droplets and particles*. CRC Press; 2011. ISBN 1439840504.
- Cui Y, Ravnik J, Hriberšek M, Steinmann P. A novel model for the lift force acting on a prolate spheroidal particle in an arbitrary non-uniform flow. Part I. Lift force due to the streamwise flow shear. *Int J Multiph Flow* 2018;104:103–12. doi:10.1016/j.ijmultiphaseflow.2018.03.007.
- Cui Y, Ravnik J, Hriberšek M, Steinmann P. On constitutive models for the momentum transfer to particles in fluid-dominated two-phase flows. In: *Advanced structured materials*. Springer International Publishing; 2018. p. 1–25. doi:10.1007/978-3-319-70563-7_1.
- Cui Y, Ravnik J, Verhjak O, Hriberšek M, Steinmann P. A novel model for the lift force acting on a prolate spheroidal particle in arbitrary non-uniform flow. Part II. Lift force taking into account the non-streamwise flow shear. *Int J Multiph Flow* 2019;111:232–40. doi:10.1016/j.ijmultiphaseflow.2018.12.003.
- Cui Y, Sommerfeld M. Forces on micron-sized particles randomly distributed on the surface of larger particles and possibility of detachment. *Int J Multiph Flow* 2015;72:39–52. doi:10.1016/j.ijmultiphaseflow.2015.01.006.
- Fan F-G, Ahmadi G. A sublayer model for wall deposition of ellipsoidal particles in turbulent streams. *J Aerosol Sci* 1995;26(5):813–40. doi:10.1016/0021-8502(95)00021-4.
- Feng Y, Kleinstreuer C. Analysis of non-spherical particle transport in complex internal shear flows. *Phys Fluids* 2013;25(9):091904. doi:10.1063/1.4821812.
- Gotoh T. Brownian motion in a rotating flow. *J Stat Phys* 1990;59(1–2):371–402. doi:10.1007/bf01015575.
- Harper EY, Chang I-D. Maximum dissipation resulting from lift in a slow viscous shear flow. *J Fluid Mech* 1968;33(02):209. doi:10.1017/s0022112068001254.
- Hölzer A, Sommerfeld M. Lattice Boltzmann simulations to determine drag, lift and torque acting on non-spherical particles. *Comput Fluids* 2009;38(3):572–89. doi:10.1016/j.compfluid.2008.06.001.
- Jebakumar AS, Premnath KN, Abraham J. Lattice Boltzmann method simulations of stokes number effects on particle trajectories in a wall-bounded flow. *Comput Fluids* 2016;124:208–19. doi:10.1016/j.compfluid.2015.07.020.
- Jebakumar AS, Premnath KN, Magi V, Abraham J. Fully-resolved direct numerical simulations of particle motion in a turbulent channel flow with the lattice-Boltzmann method. *Comput Fluids* 2019;179:238–47. doi:10.1016/j.compfluid.2018.11.003.
- Legendre D, Magnaudet J. The lift force on a spherical bubble in a viscous linear shear flow. *J Fluid Mech* 1998;368:81–126. doi:10.1017/s0022112098001621.
- Magnaudet J. Small inertial effects on a spherical bubble, drop or particle moving near a wall in a time-dependent linear flow. *J Fluid Mech* 2003;485:115–42. doi:10.1017/s0022112003004464.
- Magnaudet J, Takagi S, Legendre D. Drag, deformation and lateral migration of a buoyant drop moving near a wall. *J Fluid Mech* 2003;476. doi:10.1017/s0022112002002902.
- McLaughlin JB. Inertial migration of a small sphere in linear shear flows. *J Fluid Mech* 1991;224(-1):261. doi:10.1017/s0022112091001751.
- McLaughlin JB. The lift on a small sphere in wall-bounded linear shear flows. *J Fluid Mech* 1993;246(-1):249. doi:10.1017/s0022112093000114.
- Miyazaki K, Bedeaux D, Avalos JB. Drag on a sphere in slow shear flow. *J Fluid Mech* 1995;296(-1):373. doi:10.1017/s0022112095002163.
- Ouchene R, Khalij M, Arcen B, Tanière A. A new set of correlations of drag, lift and torque coefficients for non-spherical particles and large Reynolds numbers. *Powder Technol* 2016;303:33–43. doi:10.1016/j.powtec.2016.07.067.
- Pan T-W, Huang S-L, Chen S-D, Chu C-C, Chang C-C. A numerical study of the motion of a neutrally buoyant cylinder in two dimensional shear flow. *Comput Fluids* 2013;87:57–66. doi:10.1016/j.compfluid.2012.11.021.
- Saffman PG. The lift on a small sphere in a slow shear flow. *J Fluid Mech* 1965;22(02):385. doi:10.1017/s0022112065000824.
- Saffman PG. The lift on a small sphere in a slow shear flow – corrigendum. *J Fluid Mech* 1968;31(03):624. doi:10.1017/s0022112068999990.
- Sanjeevi SKP, Kuipers JAM, Padding JT. Drag, lift and torque correlations for non-spherical particles from stokes limit to high Reynolds numbers. *Int J Multiph Flow* 2018;106:325–37. doi:10.1016/j.ijmultiphaseflow.2018.05.011.
- Shi P, Rzehak R. Lift forces on solid spherical particles in unbounded flows. *Chem Eng Sci* 2019;208:115145. doi:10.1016/j.ces.2019.08.003.
- Sommerfeld M, van Wachem B, Oliemans R. *ERCOFTAC best practice guidelines: computational fluid dynamics of dispersed multi-phase flows*. ERCOFTAC; 2008.
- Spalart P, Allmaras S. A one-equation turbulence model for aerodynamic flows. In: *Proceedings of the 30th aerospace sciences meeting and exhibit*. American Institute of Aeronautics and Astronautics; 1992. <https://doi.org/10.2514/6.1992-439>.
- Stone HA. Philip saffman and viscous flow theory. *J Fluid Mech* 2000;409:165–83. doi:10.1017/s0022112099007697.
- Taylor GI. The motion of a sphere in a rotating liquid. *Proc R Soc A: Math Phys Eng Sci* 1922;102(715):180–9. doi:10.1098/rspa.1922.0079.
- Taylor GI. The motion of ellipsoidal particles in a viscous fluid. *Proc R Soc A: Math Phys Eng Sci* 1923;103(720):58–61. doi:10.1098/rspa.1923.0040.
- Tsornig SJ, Capart H, Lo DC, Lai JS, Young DL. Behaviour of macroscopic rigid spheres in lid-driven cavity flow. *Int J Multiph Flow* 2008;34(1):76–101. doi:10.1016/j.ijmultiphaseflow.2007.06.007.
- Wang J, Yu S, Luo S, Xia G, Zong L. Lift forces on axial symmetry particles rotating in a linear shear flow of a rarefied gas. *Phys Fluids* 2018;30(6):063302. doi:10.1063/1.5029944.
- Zastawny M, Mallouppas G, Zhao F, van Wachem B. Derivation of drag and lift force and torque coefficients for non-spherical particles in flows. *Int J Multiph Flow* 2012;39:227–39. doi:10.1016/j.ijmultiphaseflow.2011.09.004.